Ultrasound in Med. & Biol., Vol. 39, No. 8, pp. 1469–1481, 2013

0301-5629/$ - see front matter

http://dx.doi.org/10.1016/j.ultrasmedbio.2013.03.001

● *Original Contribution*

THE INTRAVASCULAR ULTRASOUND ELASTICITY-PALPOGRAPHY TECHNIQUE REVISITED: A RELIABLE TOOL FOR THE *IN VIVO* DETECTION OF VULNERABLE CORONARY ATHEROSCLEROTIC PLAQUES

Flavien Deleaval,* Adeline Bouvier,* Gérard Finet,† Guy Cloutier,‡ Saami K. Yazdani,§ Simon Le Floc'h,¶ Patrick Clarysse,‖ Roderic I. Pettigrew,# and Jacques Ohayon*$

*Laboratory TIMC-IMAG/DyCTiM, UJF, CNRS UMR 5525, In^{3}S, Grenoble, France; †Department of Hemodynamics and Interventional Cardiology, Hospices Civils de Lyon and Claude Bernard University Lyon1, INSERM Unit 886, Lyon, France; ‡Laboratory of Biorheology and Medical Ultrasonics, University of Montreal Hospital Research Center (CRCHUM), Montréal, QC, Canada; §Department of Mechanical Engineering, University of South Alabama, Mobile, AL 36688, USA; ¶Laboratory LMGC, CNRS UMR 5508, Université Montpellier II, Montpellier, France; ‖Laboratory CREATIS, CNRS UMR 5220, INSERM Unit 1044, Lyon, France; #Laboratory of Integrative Cardiovascular Imaging Science, National Institute of Diabetes Digestive and Kidney Diseases, National Institutes of Health, Bethesda, MD 20892, USA; and $University of Savoie, Polytech Annecy-Chambéry, Le Bourget du Lac, France

(*Received* 3 *October* 2012; *revised* 28 *February* 2013; *in final form* 2 *March* 2013)

Abstract—Critical to the detection of vulnerable plaques (VPs) is quantification of their mechanical properties. On the basis of intravascular ultrasound (IVUS) echograms and strain images, E. I. Céspedes, C. L. de Korte CL and A. F. van der Steen (Ultrasound Med Biol 2000;26:385–396) proposed an elasticity-palpography technique (E-PT) to estimate the apparent stress-strain modulus palpogram of the thick endoluminal layer of the arterial wall. However, this approach suffers from major limitations because it was developed for homogeneous, circular and concentric VPs. The present study was therefore designed to improve the E-PT by considering the anatomic shape of the VP. This improved E-PT was successfully applied to six coronary lesions of patients imaged *in vivo* with IVUS. Our results indicate that the mean relative error of the stress-strain modulus decreased from 61.02 ± 9.01% to 15.12 ± 12.57% when the IE-PT was used instead of the E-PT. The accuracy of the stress-strain modulus palpograms computed using the improved theoretical framework was also investigated with respect to noise, which may affect prediction of plaque vulnerability. (E-mail: jacques.ohayon@imag.fr) © **2013 World Federation for Ultrasound in Medicine & Biology.**

Key Words: **Atherosclerosis, Vulnerable plaques, Elastography, Coronary disease, Inverse problem.**

INTRODUCTION

Vulnerable atherosclerotic plaque (VP) rupture is the leading cause of acute coronary syndrome, myocardial infarction and stroke in the Western world (Lloyd-Jones et al. 2010). Morphologically, an unstable vulnerable coronary lesion consists of a relatively large extracellular necrotic core with a thin fibrous cap (<65 μm) infiltrated by macrophages (Virmani et al. 2000). The thin-cap fibroatheroma is the precursor lesion, which, once ruptured, may lead to the formation of a thrombus causing an acute syndrome and possibly death (Virmani et al. 2006). Several intravascular (IV) techniques are used to detect coronary VPs in clinics (Vancraeynest et al. 2011), including ultrasound (IVUS) (Carlier and Tanaka 2006; Rioufol et al. 2002), optical coherence tomography (OCT) (Jang et al. 2002; Tearney et al. 2008) and magnetic resonance imaging (IVMRI) (Briley-Saebo et al. 2007; Larose et al. 2005). Diagnosing unstable VPs, on the other hand, is still imprecise, as the thickness of the fibrous cap alone is not a sufficient predictor of plaque stability (Fleg et al. 2012; Maldonado et al. 2012; Ohayon et al. 2008; Virmani et al. 2000). Biomechanical studies have identified peak cap stress amplitude as an additional key predictor of vulnerability to rupture (Finet et al. 2004; Loree et al. 1992; Ohayon et al. 2001).

Quantifying intraplaque stress distribution, to predict plaque rupture, has been a challenge. To overcome this hurdle, the local deformation (strain) of a tissue can be

Address correspondence to: Jacques Ohayon, Laboratory TIMC-IMAG/DyCTiM, UJF, CNRS UMR 5525, In^{3}S, Grenoble, France. E-mail: jacques.ohayon@imag.fr

Conflicts of Interest: The authors have indicated that they have no conflicts of interest regarding the content of this article.

calculated and can then be directly related to the intraplaque stress and its mechanical properties. Ophir and colleagues (Ophir et al. 1991; Céspedes et al. 1993) were the pioneers in developing imaging techniques based on the strain field. On the basis of their work, several elegant IVUS methods were developed to highlight spatial strain distribution (*i.e.,* strain elastogram) over the entire vessel wall (Maurice et al. 2007) or over a restricted thick endoluminal region (de Korte et al. 2002; Doyley et al. 2001). Such IVUS techniques based on optical flow (Maurice et al. 2004) or time-delay correlation estimation (de Korte et al. 2002) allowed calculations of intraplaque strain images during the cardiac cycle.

These methods did not, however, overcome a main limitation related to the complex geometries of atherosclerotic plaques, which alter intraplaque strain fields and inhibit direct translation into plaque mechanical properties. Therefore, to complement the characterization of an atherosclerotic lesion from an IVUS echogram and strain images, Céspedes et al. (2000) developed an elegant one-dimensional elasticity-palpography technique (E-PT) to estimate and display an apparent local stiffness (called the *stress-strain modulus* [S-SM] *palpogram*) of the thick endoluminal layer of the arterial wall (called the *palpography domain*). Although such work presents promising concepts for the identification of atherosclerotic lesions, current E-PT suffers from major limitations. First, the mechanical solution used to extract the S-SM palpogram was obtained by assuming a cylindrical concentric arterial wall made of a homogeneous isotropic incompressible medium and submitted to a uniform outer radial stress distribution (Timoshenko and Goodier 1987). Second, with such a simplified model, it is difficult to correlate the resulting S-SM to the real Young's modulus distribution in the palpography domain. Such a solution is too restrictive and must be used with caution in atherosclerotic lesions with high eccentricity and non-uniform wall thickness.

The present biomechanical study was designed to improve the theoretical framework of the E-PT by considering the anatomic shape of the atherosclerotic coronary artery. This improved elasticity-palpography technique (IE-PT), based on the continuum mechanics theory prescribing the strain field in the palpography region, was successfully applied to six coronary lesions of patients imaged *in vivo* with IVUS. The robustness and performance of the new IE-PT were investigated with respect to noise, which may affect prediction of plaque vulnerability.

METHODS

Six patients underwent coronary IVUS, and the extracted plaque geometries were used to simulate strain fields for which the performance of the improved elasticity-palpography technique was tested. Moreover, one idealized eccentric and circular non-vulnerable plaque geometry with a homogeneous lesion was designed to highlight the main limitations of the original E-PT.

Intravascular ultrasound study and plaque geometries

Patient population. Arteries of patients referred for percutaneous coronary intervention at the Lyon Cardiology Hospital (Hôpital Cardiologique et Pneumologique de Lyon, France) after a first acute coronary syndrome with troponin I elevation were explored. Investigations were approved by the institutional board of the hospital's cardiology department, and consent was obtained from the patients.

IVUS imaging. Non-ruptured VP geometries were obtained from IVUS scans of the coronary arteries using the protocol described by Rioufol et al. (2002). To avoid vasospasms, IVUS exploration was performed after intracoronary administration of 200 μg of nitroglycerine. The acquired cross-sectional IVUS image of the VP corresponded to the site exhibiting the thinner fibroatheroma cap. IVUS scans were performed with the iLab platform (Boston Scientific, Watertown, MA, USA) equipped with 40-MHz catheters (Atlantis SR Pro 3.6F, Boston Scientific). The spatial resolution of the ultrasound images acquired with the IVUS system was approximately 90 μm in the radial direction (Chopard et al. 2010).

IVUS image analysis. IVUS echogenicity aspects were used to characterize VP components: (i) highly hypoechogenic components (or anechogenic zones), suggestive of quasi-cellular tissues (lipid or cellular deposition); (ii) homogeneous reflective components, suggestive of organized or disorganized fibrosis; or (iii) hyperechogenic components (or bright zones), suggestive of calcified regions (Di Mario et al. 1998). A manual segmentation procedure using ImageJ software (ImageJ, NIH, Bethesda, MD, USA) was performed by a cardiologist to extract the contours of each plaque component.

IVUS measurements and definitions. Each cross-sectional IVUS image of a lesion was quantitatively analyzed. Plaque area (Pla_{area}, mm^2); lumen area (Lu_{area}, mm^2); necrotic core area ($Core_{area}$, mm^2); calcified area (Cal_{area}, mm^2); degree of stenosis ($Stenos_{deg}$, %), which is $100 \times Pla_{area} / (Pla_{area} + Lu_{area})$; and cap thickness ($Cap_{thick}$, mm), which is defined as the shortest distance between the lumen and the necrotic core, were measured.

Forward problem: Strain field distributions

The files of the digitized contours obtained with ImageJ were imported into MATLAB and then transferred in Comsol (Structural Mechanics Module, Version 3.5,

Comsol, France) *via* the LiveLink MATLAB/Comsol toolbox. Radial strain elastograms were obtained by performing static finite-element (FE) computations on all VP geometries using Comsol software. Entire plaque geometries were meshed with approximately 15,000 six-node triangular elements. The center of gravity of the lumen, which was numerically determined as the barycenter (*i.e.,* the center of mass) of the lumen area, was used as the origin of the cylindrical coordinate system(r, θ). The strain fields were interpolated on a regular polar mesh with a given radial step resolution of 36 μm and an angular step resolution corresponding to 256 radial directions, which is the resolution that can be expected from endovascular elastography (Maurice et al. 2007).

Boundary conditions and material properties. The FE simulations were conducted under the assumption of plane strain. Because instantaneous pressure was not recorded during IVUS scans of the coronary arteries, we assumed a blood pressure differential, ΔP, of 1 kPa (or 7.5 mm Hg), which corresponds to a realistic pressure gradient occurring between two successive IVUS images recorded during the cardiac cycle. Free boundary condition was assumed at the external diameter of the artery. The mechanical properties of the fibrosis, calcified area and soft necrotic core were modeled as isotropic and quasi-incompressible media (Poisson ratio $\nu = 0.49$) with Young's moduli $E_{\text{fibrosis}} = 800$ kPa, $E_{\text{calcified}} = 5000$ kPa and $E_{\text{core}} = 5$ kPa, respectively (Finet et al. 2004).

Sensitivity study of effect of noise on input radial strain data. To investigate the influence of noise on the performance of the improved elasticity-palpography technique, white noise was added to each FE simulated radial strain field used as input. For the noise model, we used a normal distribution of noise with zero mean and a standard deviation of $(a\varepsilon_{rr} + b)\beta$, where $a = 0.2\%$, $b = 0.04\%$ and ε_{rr} is the local value of the radial strain (Baldewsing et al. 2005; Le Floc'h et al. 2009). The noise field was significantly amplified by increasing β from 1 to 6. For each level of noise β, 10 computations in which the noise was spatially randomly distributed were performed, and the averaged Young's modulus of each plaque constituent ($\pm$ standard deviation) was presented.

Inverse problem: Stress-strain modulus palpogram

Stress-strain modulus palpogram of Céspedes et al. (2000). The S-SM (called E_{palpo}) was defined by Céspedes et al. (2000) as the local radial stiffness of the thick endoluminal layer of the arterial wall (*i.e.,* of the palpography domain). Inspired by the expression of the S-SM obtained for a thick-walled isotropic cylindrical vessel with a specific concentric cylindrical palpography domain, Céspedes et al. (2000) proposed the S-SM approximation (all details are presented in Appendix I)

$$E_{\text{palpo}}^{\text{Céspedes}}(\theta) = \frac{\Delta P/2}{\varepsilon(\theta)} \tag{1a}$$

$$\varepsilon(\theta) = \left| \int_{R_i(\theta)}^{R_p(\theta)} \varepsilon_{rr}(r, \theta) dr \right| \tag{1b}$$

where $R_i(\theta)$ and $R_p(\theta)$ are the inner and outer radii of the palpography domain, respectively.

Stress-strain modulus palpogram revisited. We revisited the S-SM formulation of Céspedes et al. (2000) to account for both the anatomic shapes of the atherosclerosis plaque and the palpography domain. On the basis of the relationship between the deviatoric radial stress $\sigma_{rr}^{\text{dev}}(r, \theta)$, the Young's modulus $E(r, \theta)$ and the radial strain component $\varepsilon_{rr}(r, \theta)$ for a heterogeneous, isotropic, incompressible and linear elastic continuum medium (Timoshenko and Goodier 1987),

$$\sigma_{rr}^{\text{dev}}(r, \theta) = \frac{2}{3} E(r, \theta) \varepsilon_{rr}(r, \theta) \tag{2}$$

we redefined the S-SM as the ratio of the average deviatoric radial stress to the average radial strain along the radial axis

$$E_{\text{palpo}}^{new}(\theta) = \frac{3}{2} \frac{\left| \int_{R_i(\theta)}^{R_p(\theta)} \sigma_{rr}^{\text{dev}}(r, \theta) dr \right|}{\varepsilon(\theta)} \tag{3}$$

where $\varepsilon(\theta)$ is given by Eq. (1b).

Moreover, knowing that the radial strain $\varepsilon_{rr}(r, \theta)$ is proportional to the imposed change in pressure, ΔP, and inversely proportional to the amplitude of the Young's modulus, $E(r, \theta)$,

$$\varepsilon_{rr}(r, \theta) = \frac{3}{2} \frac{\Delta P}{E(r, \theta)} h(r, \theta) \tag{4}$$

(where the constant 3/2 is introduced for mathematical convenience only), the expression of the deviatoric radial stress given by Eq. (2) can be rewritten as

$$\sigma_{rr}^{\text{dev}}(r, \theta) = \Delta P \; h(r, \theta) \tag{5}$$

where $h(r, \theta)$ is a new correcting shape function that accounts for the entire plaque morphology, including the geometries of all plaque heterogeneities. Taking advantage of such an expression for the deviatoric radial stress, the new S-SM (Eq. [3]) becomes

Table 1. IVUS-detected and modeled atherosclerotic plaque characteristics

Plaque no.	Origin of geometry	Cap thickness (μm)	Area (mm^2)				Stenosis (%)
			Necrotic core	Calcium	Plaque	Lumen	
1	Model	—	—	—	25.13	3.14	89
2	IVUS	93	1.36	—	8.74	2.789	76
3	IVUS	100	5.39	—	16.70	3.24	84
4	IVUS	162	1.20/0.51	—	17.85	6.75	73
5	IVUS	193	2.11	0.40	17.53	3.60	83
6	IVUS	62	3.54	1.60	15.64	4.52	78
7	IVUS	220	2.15/0.70	0.89	16.88	3.62	82

IVUS = intravascular ultrasound.

$$E^{new}_{\text{palpo}}(\theta) = \frac{\Delta P \left| \int_{R_i(\theta)}^{R_p(\theta)} h(r,\theta)dr \right|}{\varepsilon(\theta)} \qquad (6)$$

Because $h(r, \theta)$, is an unknown function that escapes to direct measurements, we computed an approximated correcting shape function, $h^*(r, \theta)$, that accounts for anatomic cross-sectional plaque geometry. Such an approximated correcting function was obtained by using a FE analysis and by assuming the plaque homogeneous, isotropic and quasi incompressible with the Young's modulus E. This FE simulation was performed in linear elasticity with a loading blood pressure amplitude ΔP. From Eq. (4) and with the knowledge of the spatial radial strain distribution, we extracted the approximated shape function, $h^*(r, \theta)$, which was used to revisit the S-SM formulation for complex plaque geometries:

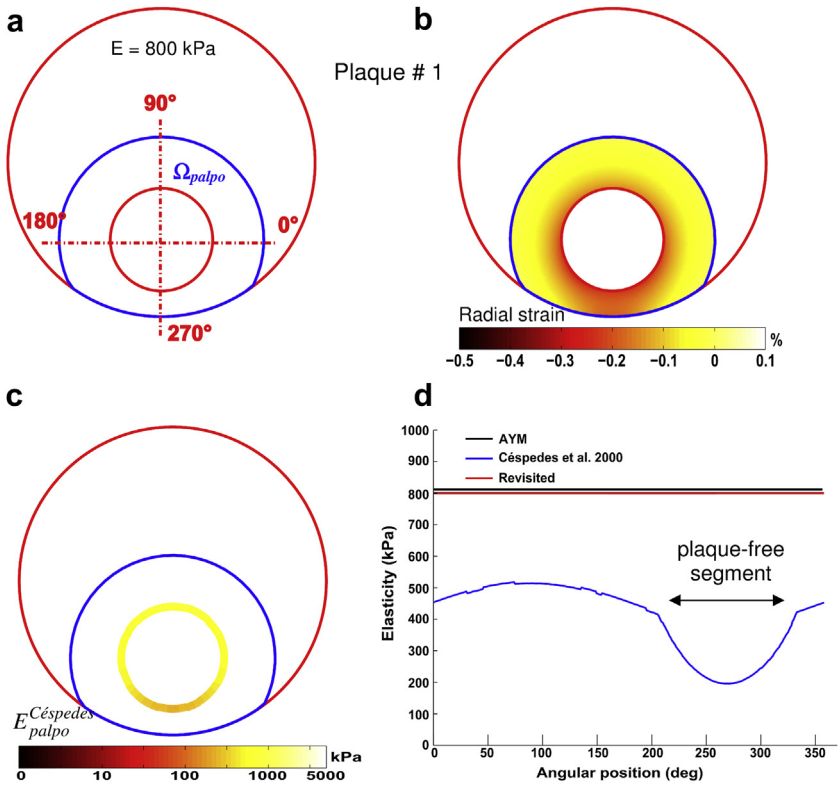

Fig. 1. Performance of the improved elasticity-palpography technique. (a) Contours (in red) of an idealized eccentric and circular plaque model (called plaque 1) in which the lesion is homogeneous. The palpography domain, Ω_{palpo}, is also given (blue contours). (b) Radial strain elastogram computed in the palpography domain. (c) Computed original (Céspedes et al. 2000) stress-strain modulus (S-SM) palpogram. (d) Comparisons between original S-SM, improved (Revisited) S-SM and averaged Young's modulus (AYM) palpograms.

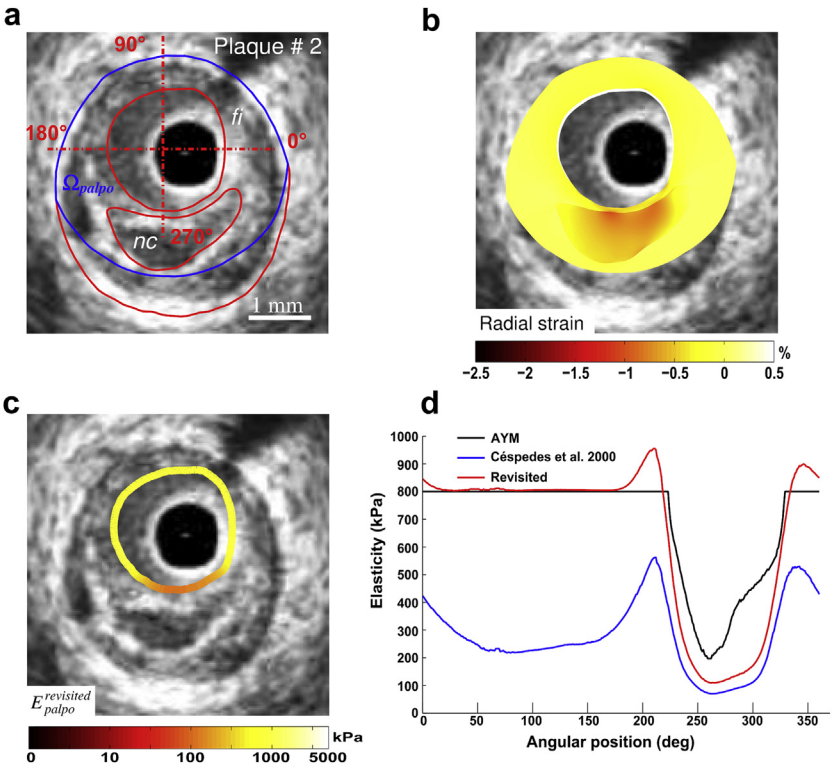

Fig. 2. Performance of the improved elasticity-palpography technique in detecting a vulnerable plaque when the whole necrotic core is included in the palpography domain. (a) Intravascular ultrasound image of plaque 2 with plaque constituents (red contours). The boundaries of the palpography domain, Ω_{palpo}, are also given (blue contours). (b) Radial strain elastogram in the palpography domain. (c) Computed improved (Revisited) stress-strain modulus (S-SM) palpogram. (d) Comparisons between original S-SM (Céspedes et al. 2000), improved (Revisited) S-SM and averaged Young's modulus (AYM) palpograms. nc = necrotic core, fi = fibrous region.

$$E^{\text{revisited}}_{\text{palpo}}(\theta) = \frac{\Delta P \left| \int_{R_i(\theta)}^{R_p(\theta)} h^*(r,\theta)dr \right|}{\varepsilon(\theta)} \quad (7)$$

Interestingly, this original revisited S-SM formulation (Eq. [7]) allows us to find the real Young's modulus amplitude E when considering a homogeneous isotropic plaque (*i.e.*, $E^{\text{revisited}}_{\text{palpo}}(\theta) = E$), whatever their geometries and the palpography domains considered Ω_{palpo}, where $R_i(\theta) \leq r \leq R_p(\theta)$.

The Young's modulus palpogram. To discuss the physical meaning of the original and revisited S-SM formulations given by Eqs. (1) and (7), respectively, we compared them with the circumferential distribution of the averaged Young's modulus along the radial axis (AYM):

$$\text{AYM}(\theta) = \frac{1}{R_p(\theta) - R_i(\theta)} \int_{R_i(\theta)}^{R_p(\theta)} E(r,\theta)dr \quad (8)$$

where $E(r,\theta)$ is the spatial distribution of the Young's modulus.

Moreover, to quantify the accuracy of the reconstructed S-SM palpograms we computed the mean relative stress-strain modulus error (MR_{error}):

$$MR_{error} = 100 \int_0^{2\pi} \frac{E_{palpo}(\theta) - AYM(\theta)}{AYM(\theta)} d\theta \quad (9)$$

RESULTS

Intravascular ultrasound study

Six non-ruptured VPs with necrotic cores and calcified areas were identified after extensive IVUS scanning. The geometric characteristics of the six non-ruptured VPs scanned *in vivo* (plaques 2–7) and the eccentric circular idealized homogeneous plaque (plaque 1) are summarized in Table 1. All results presented in our figures were obtained from simulations performed without white noise (*i.e.*, $\beta = 0$) and with a blood pressure differential, ΔP, of 1 kPa, unless otherwise stated.

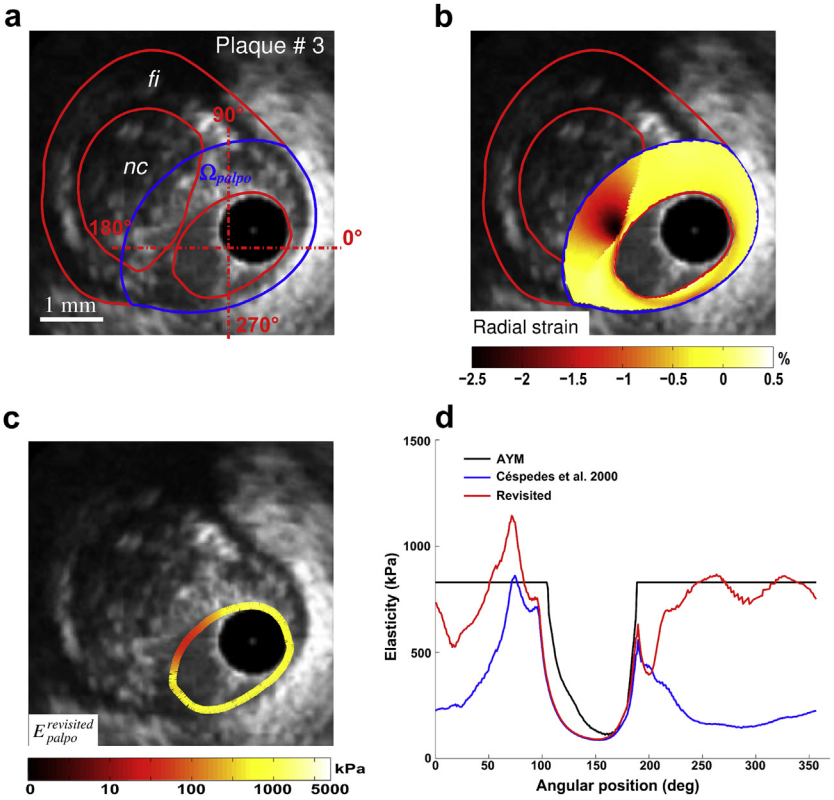

Fig. 3. Performance of the improved elasticity-palpography technique in detecting a vulnerable plaque when only a part of the large necrotic core is included in the palpography domain. (a) Intravascular ultrasound image. (b) Radial strain. (c) Improved (Revisited) stress-strain modulus (S-SM) palpogram. (d) Comparisons between S-SM palpograms.

Performance of improved elasticity-palpography technique

Importance of considering the correcting stress function. To highlight the importance of using the revisited S-SM formulation for non-concentric lesions with arbitrary palpography domains, we first conducted our simulations on the idealized eccentric plaque geometry (see plaque 1, Fig. 1). This idealized homogeneous plaque was assumed to be isotropic (E = 800 kPa) and quasi-incompressible (Poisson ratio v = 0.49). The improved S-SM palpogram appears to be less sensitive to the geometries of the arterial plaque and palpography domain than that derived with the E-PT. The S-SM palpogram computed with the IE-PT remains almost constant and close to 800 kPa-which is also the value of the real averaged Young's modulus-even in the free-plaque arc length, which is the thinnest region of the palpography domain (Fig. 1d).

Detection of soft inclusions. Improved S-SM palpograms obtained for VPs with one (plaques 2 and 3, Figs. 2 and 3) and two (plaque 4, Fig. 4) necrotic cores are illustrated. Necrotic core sites were accurately detected using the IE-PT. The amplitude of the revisited S-SM was found to be close to the Young's modulus of the fibrosis (*i.e.*, close to 800 kPa) excepted at a soft inclusion locations, for which the S-SM amplitudes were found to be lower. Compared with the AYM, the S-SM values at the necrotic core locations were underestimated.

Detection of vulnerable plaques with calcified inclusions. For two VP morphologies (plaques 5 and 6) with isolated necrotic cores and calcified inclusions (Figs. 5 and 6), the IE-PT detected and differentiated the soft and hard inclusions. Compared with the AYM, the S-SM amplitudes at the calcified inclusion locations were underestimated by almost a factor of 2. Figure 7 illustrates the abilities of the proposed IE-PT to detect a complex VP (plaque 7) with adjacent soft and hard inclusions located between 7 and 9 o'clock and one isolated large necrotic core located between 2 and 6 o'clock. The IE-PT successfully detected the isolated soft inclusion adjacent to the calcified area.

Comparison between original and improved elasticity-palpography techniques. Our quantitative results indicated that the mean relative error of the stress-strain modulus decreased from 61.02±9.01% to 15.12±12.57% when using the improved rather than the original elasticity-palpography technique (see

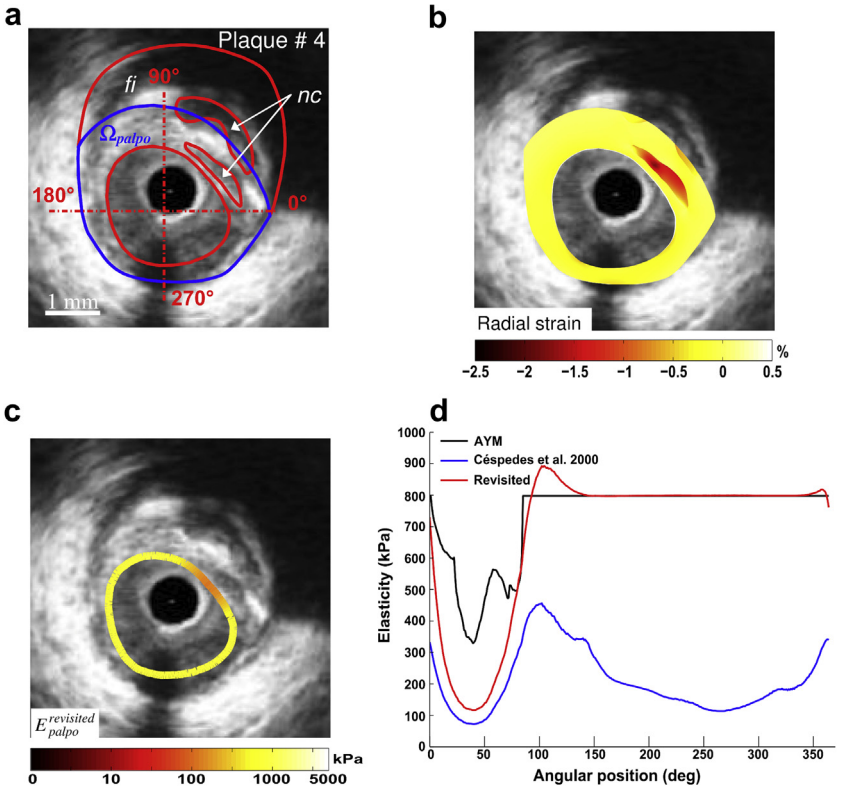

Fig. 4. Performance of the improved elasticity-palpography technique in detecting a vulnerable plaque with two necrotic cores. (a) Intravascular ultrasound image. (b) Radial strain. (c) Improved (Revisited) stress-strain modulus (S-SM) palpogram. (d) Comparisons between S-SM palpograms.

Table 2). Simulations performed on plaque 4 (Fig. 4) using the original palpography approach did not differentiate the geometric effects induced by the shape of the VP from those generated by the mechanical properties of heterogeneous plaque (Fig. 4d). When the E-PT of Céspedes et al. (2000) was used, the S-SM amplitudes computed along the plaque-free segment (*i.e.,* between angular positions 180° and 300°, Fig. 4a, d) were found to be similar to those computed at the plaque segment with necrotic cores (*i.e.,* between 0° and 90°, Fig. 4a, d). The IE-PT corrected for such geometric effects because the improved S-SM palpogram highlighted the soft inclusion site only. Similar results were found for all VPs considered in this study (see Figs. 2, 3 and 5).

Influence of white noise on stress-strain modulus palpogram. The influence of noise was studied on vulnerable plaque 2 (Fig. 8 and Table 2). Based on the definition of the signal-to-noise ratio, we converted our white noise amplitude on the decibel scale (see Appendix II). By applying such an approach to plaque 2, we found that $\beta = 2$, 4 and 6 corresponds to noise levels of 13, 7 and 3.4 dB, respectively. The robustness of the IE-PT with increasing white noise level is illustrated in Figure 8. According to the simulations performed, even on introduction of significant white noise ($\beta = 6$), the IE-PT was still able to detect the soft inclusion site (Fig. 8c). We found that the mean relative error of the stress-strain modulus MR_{error} increased from 4.70 ± 4.90% at a white noise level of $\beta = 2$ to 26.18 ± 16.24% at triple the white noise ($\beta = 6$) (Table 2).

DISCUSSION

Critical to the detection of VPs is accurate quantification of both the morphology and the mechanical properties of the diseased arteries (Cheng et al. 1993; Finet et al. 2004). Such knowledge could lead to development of a specific therapy for prevention of acute thrombotic events (Libby 2001). Although several endovascular approaches have been implemented to approximate mechanical strain *in vivo* (de Korte et al. 2002; Doyley 2012; Kim et al. 2004; Maurice et al. 2007; Wan et al. 2001), the spatial plaque Young's modulus has not yet been determined for "real-time" clinical use. Such an elasticity map remains difficult to assess because the full inverse problem needs to be solved in continuum mechanics using sophisticated non-linear mathematical optimization tools and complex procedures (Doyley

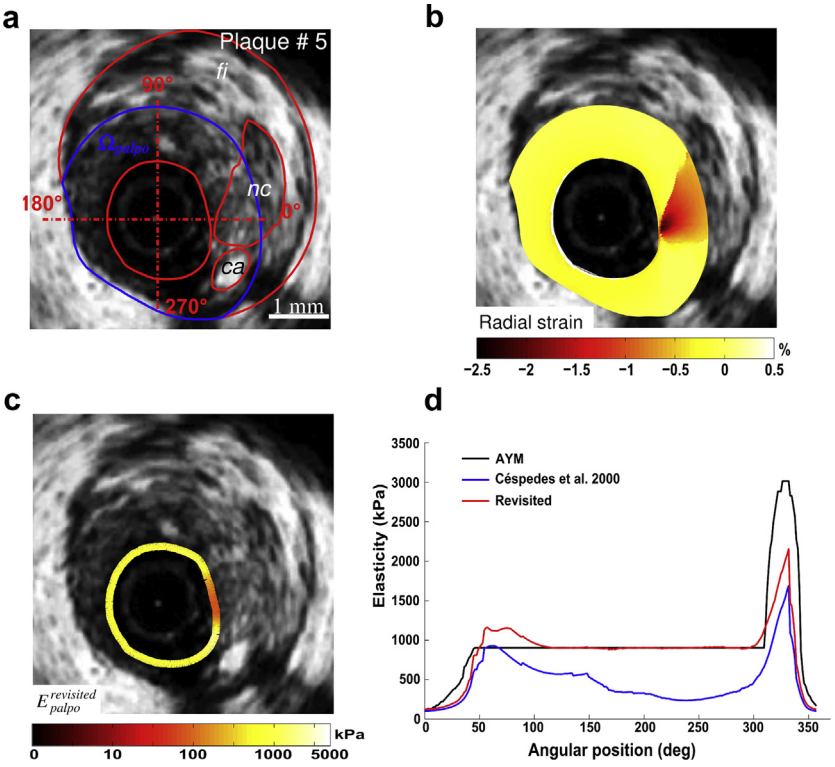

Fig. 5. Performance of the improved elasticity-palpography technique in detecting a vulnerable plaque with a small calcified inclusion. (a) Intravascular ultrasound image. (b) Radial strain. (c) Improved (Revisited) stress-strain modulus (S-SM) palpogram. (d) Comparisons between S-SM palpograms.

2012; Le Floc'h et al. 2009, 2010, 2012; Richards and Doyley 2011;).

Céspedes et al. (2000) proposed the E-PT, which allows rapid quantification of wall stiffness on the basis of arterial strain and blood pressure measurements. However, this technique suffers from major limitations because it was developed for homogeneous, isotropic, quasi incompressible, circular and concentric atherosclerotic plaques only. Therefore, in the present study, the original palpography technique was successfully revisited and improved to account for complex plaque and arbitrary palpography domain geometries.

Our results clearly indicate that the performance of the revisited S-SM formulation not only significantly improved the accuracy of the original S-SM palpogram, but, more importantly, gave physical meaning to the amplitude of the improved S-SM palpogram.

Has the revisited stress-strain modulus formulation significantly improved the palpography technique?

The original S-SM palpogram neglected the geometric effects induced by the anatomic shape of the atherosclerotic plaque and was derived on the assumption of a circular palpography domain. When the E-PT was used, the resulting S-SM values along the plaque-free segment of the atherosclerotic coronary artery were found to be lower than the averaged Young's modulus amplitudes of the arterial wall. The original S-SM palpogram of plaque 2 (Fig. 2d) shows such sites with low S-SM amplitudes located between angular positions 50° and 150° (Fig. 2a and c). The IE-PT corrects for this limitation as it accounts for real plaque and palpography domain geometries. Moreover, simulations performed on the idealized homogeneous lesion (plaque 1) (Fig. 1) clearly illustrate the advantage of considering the new approach. Indeed, the exact solution was reached when using the revisited technique, whereas the mean relative error was close to 49% when the original technique was used (Table 2). The IE-PT is less sensitive to geometric effects and can differentiate between plaque elasticity and apparent stiffness, which is dependent on arterial wall thickness (Fig. 1).

Is the stress-strain modulus palpogram sufficient to detect vulnerable plaques?

The IE-PT is sufficient to detect and identify all VPs without calcified inclusions (see Figs. 2, 3 and 4). More interestingly, the IE-PT appears to be reliable enough to detect complex VPs with calcified inclusions (Figs. 5, 6 and 7). Let us point out that although both S-SM palpograms for plaque 7 (Fig. 7c), correctly identified the presence of the necrotic core, even though a soft

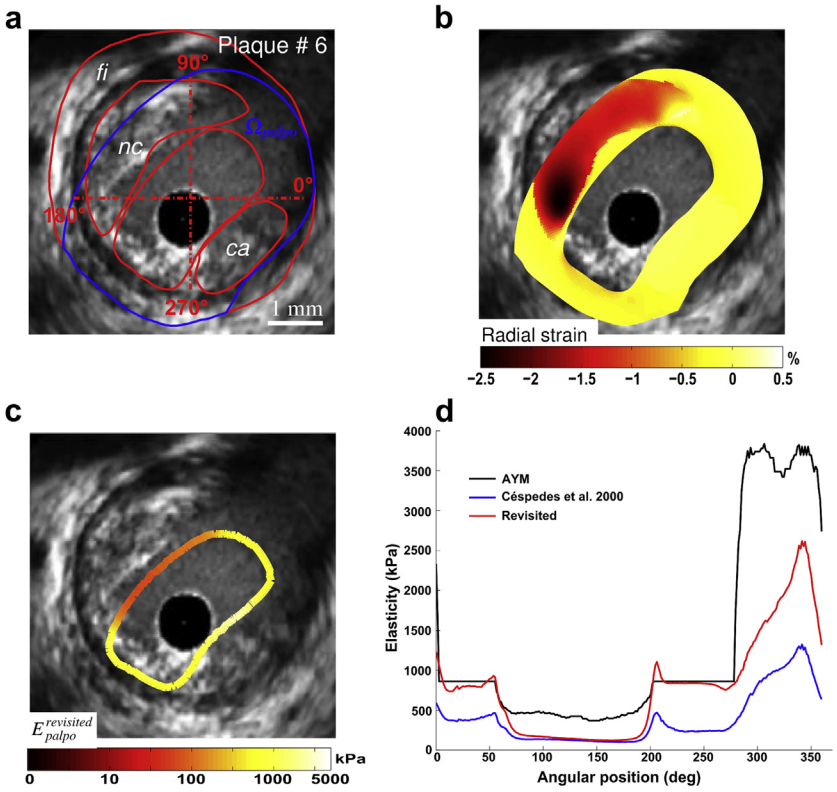

Fig. 6. Performance of the improved elasticity-palpography technique in detecting vulnerable plaque with a large calcified area. (a) Intravascular ultrasound image. (b) Radial strain. (c) Improved (Revisited) stress-strain modulus (S-SM) palpogram. (d) Comparisons between S-SM palpograms.

inclusion was adjacent to the calcified inclusion and increased the amplitude of the AYM at this site (*i.e.*, between angular positions 180° and 240°) (Figs. 7a, d), only the IE-PT was able to correct for the elasticity amplitudes at the plaque-free segment (*i.e.*, between angular positions 30° and 180°) (Fig. 7a, d).

Is the revisited stress-strain modulus palpogram sufficient to diagnose the degree of stability of vulnerable plaques?

Fibrous cap thickness is often used by interventional cardiologists to diagnose the degree of VP instability. Recent studies (Cilla et al. 2012; Ohayon et al. 2008) have shown that other emergent biomechanical factors such as necrotic core thickness (rather than necrotic core area) and arterial remodeling index are also critical in determining plaque instability. The palpography technique does not permit direct measurements of such key morphologic determinants. Therefore, although the IE-PT is reliable in detecting VPs, this approach is not sufficient to diagnose the degree of stability of VPs.

Is there an optimal size for the palpography domain?

As mentioned previously, the main limitation of the palpography technique is that an optimal circular palpography domain is necessary to obtain accurate and reliable S-SM palpograms. Thus, the original S-SM appears to be more adaptable to the detection of vulnerable concentric atherosclerotic lesions, because its formulation was based on the assumption of a cylindrical concentric plaque. The IE-PT may be viewed as an extension of the original formulation allowing the detection of eccentric VPs, which are very common (Glagov et al. 1987). Furthermore, the cardiologist has the flexiblity to choose any arbitrary endoluminal thick layer size and shape as the palpography domain.

Study limitations

A major limitation of this study was that our analysis was performed in the absence of residual strain. The effects of such residual strain have been investigated in an *ex vivo* study performed by Ohayon et al. (2007) with several human vulnerable coronary plaque samples. We found that residual strain was not negligible and affects mainly the peak cap stress amplitude in the thin fibrous cap. Therefore, on the basis of our previous findings, the absence of residual strain should not alter the characterization of the mechanical properties presented in this study, which was the ultimate goal.

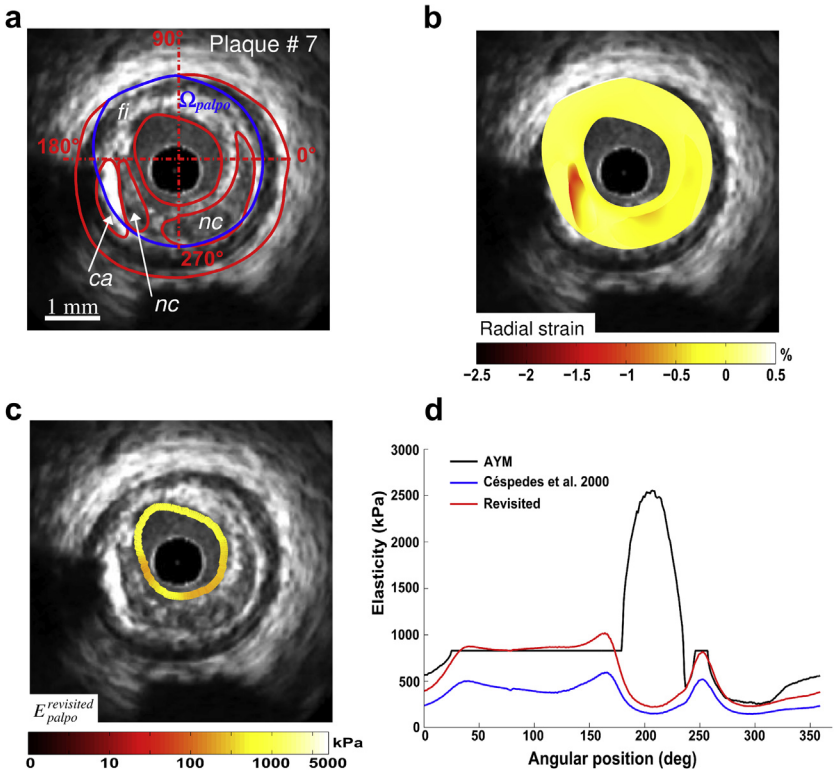

Fig. 7. Performance of the improved elasticity-palpography technique in detecting a vulnerable plaque with a small calcified inclusion adjacent to a necrotic core. (a) Intravascular ultrasound image. (b) Radial strain. (c) Improved (Revisited) stress-strain modulus (S-SM) palpogram. (d) Comparisons between S-SM palpograms.

A second study limitation was that our study was performed on a relatively small number of cases ($n = 7$). Such atherosclerotic lesions were chosen to be representative of a larger population. Indeed, different necrotic core and calcified inclusion shapes were used to take into account a large variety of clinical cases. Nevertheless, further studies are needed to extend and strengthen the present findings.

Potential clinical implication

Stabilization of vulnerable plaque remains a significant clinical problem (Abela et al. 2011; Ylä-Herttuala et al. 2011). Studies conducted to analyze the structural variation in the fibrous cap and necrotic core with specific drug treatments (*e.g.,* all statins, angiotensin-converting enzyme inhibitors) revealed an enhancement of plaque stability (Libby et al. 2002; Nozue et al. 2012). As shown

Table 2. Mean relative errors (MR_{error}) obtained from palpograms when using either the original or improved elasticity-palpography technique*

		Improved (revisited) MR_{error} (%)			
			With noise		
Plaque no.	Original MR_{error} (%) without noise	Without noise ($\beta = 0$)	$\beta = 2$	$\beta = 4$	$\beta = 6$
1	48.97	0.00	—	—	—
2	60.82	11.43	4.70 ± 4.90	14.52 ± 12.46	26.18 ± 16.24
3	61.70	17.30	—	—	—
4	71.26	10.89	—	—	—
5	55.49	8.21	—	—	—
6	73.97	40.18	—	—	—
7	54.89	17.85	—	—	—
	61.02 ± 9.01	15.12 ± 12.57	—	—	—

* The influence of white noise was studied using vulnerable plaque 2.

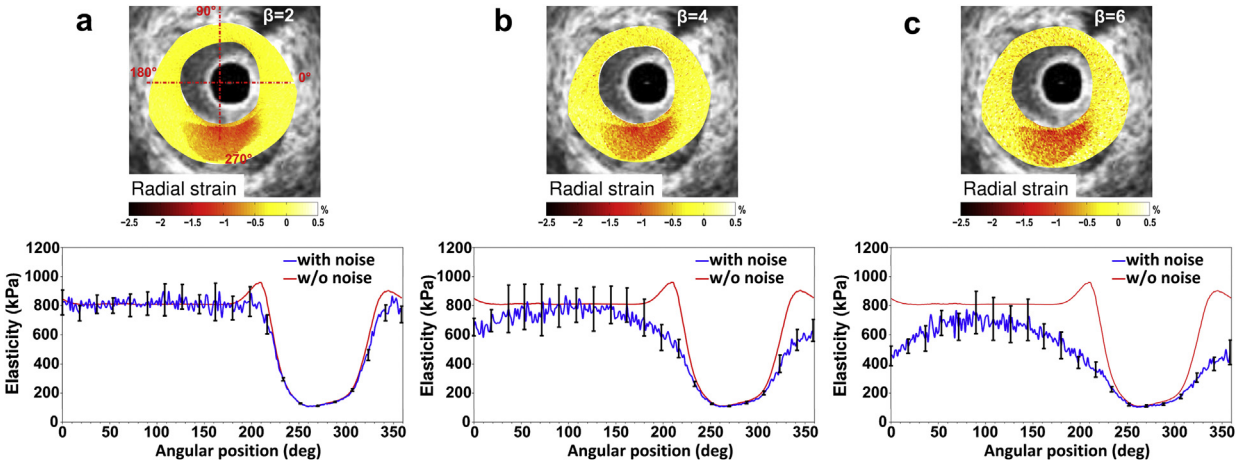

Fig. 8. Results of the sensitivity analysis performed to investigate the influence of white noise added to the strain field on the reconstructed improved stress-strain modulus (S-SM) palpogram. Plaque 2 was used for this study. Row 1: Input radial strain fields obtained with different levels of white noise (β = 2, 4 and 6). Row 2: S-SM palpograms obtained with the improved elasticity-palpography technique.

in one of our previous studies (Finet et al. 2004), a very slight increase in the mechanical properties of plaque constituents, namely, hardening of the lipidic necrotic core, can tilt a VP from instability to stability. The proposed improved elasticity-palpography imaging technique is promising because it provides a non-invasive approach to analyze the evolution of the mechanical properties of atherosclerotic plaques during drug therapies.

Acknowledgments—Grant support was provided by the Agence Nationale de la Recherche (ANR), France (ATHEBIOMECH project), and by the collaborative health research joint program of the Natural Sciences and Engineering Research Council of Canada (NSERC 323405–06) and the Canadian Institutes of Health Research (CIHR CPG-80085). This research is now supported by a joint international program of the ANR (MELANII Project 09-BLANC-0423) and NSERC Strategic Grant STPGP-381136–09. Flavien Deleaval held a doctoral fellowship from la Région Rhône-Alpes, France (2010–2013).

REFERENCES

Abela GS, Vedre A, Janoudi A, Huang R, Durga S, Tamhane U. Effect of statins on cholesterol crystallization and atherosclerotic plaque stabilization. Am J Cardiol 2011;107:1710–1717.

Baldewsing RA, Mastik F, Schaar JA, Serruys PW, van der Steen AF. Robustness of reconstructing the Young's modulus distribution of vulnerable atherosclerotic plaques using a parametric plaque model. Ultrasound Med Biol 2005;31:1631–1645.

Briley-Saebo KC, Mulder WJ, Mani V, Hyafil F, Amirbekian V, Aguinaldo JG, Fisher EA, Fayad ZA. Magnetic resonance imaging of vulnerable atherosclerotic plaques: Current imaging strategies and molecular imaging probes. J Magn Reson Imaging 2007;26: 460–479.

Carlier SG, Tanaka K. Studying coronary plaque regression with IVUS: A critical review of recent studies. J Interv Cardiol 2006;19:11–15.

Cespedes EI, de Korte CL, van der Steen AF. Intraluminal ultrasonic palpation: Assessment of local and cross-sectional tissue stiffness. Ultrasound Med Biol 2000;26:385–396.

Cespedes I, Ophir J, Ponnekanti H, Maklad N. Elastography: Elasticity imaging using ultrasound with application to muscle and breast in vivo. Ultrason Imaging 1993;15:73–88.

Cheng GC, Loree HM, Kamm RD, Fishbein MC, Lee RT. Distribution of circumferential stress in ruptured and stable atherosclerotic lesions: A structural analysis with histopathological correlation. Circulation 1993;87:1179–1187.

Chopard R, Boussel L, Motreff P, Rioufol G, Tabib A, Douek P, Meyronet D, Revel D, Finet G. How reliable are 40 MHz IVUS and 64-slice MDCT in characterizing coronary plaque composition? An ex vivo study with histopathological comparison. Int J Cardiovasc Imaging 2010;26:373–383.

Cilla M, Pena E, Martinez MA. 3D computational parametric analysis of eccentric atheroma plaque: Influence of axial and circumferential residual stresses. Biomech Model Mechanobiol 2012;11: 1001–1013.

De Korte CL, Carlier SG, Mastik F, Doyley MM, van der Steen AF, Serruys PW, Bom N. Morphological and mechanical information of coronary arteries obtained with intravascular elastography: Feasibility study in vivo. Eur Heart J 2002;23:405–413.

Di Mario C, Gorge G, Peters R, Kearney P, Pinto F, Hausmann D, von Birgelen C, Colombo A, Mudra H, Roelandt J, Erbel R. Clinical application and image interpretation in intracoronary ultrasound. Study Group on Intracoronary Imaging of the Working Group of Coronary Circulation and of the Subgroup on Intravascular Ultrasound of the Working Group of Echocardiography of the European Society of Cardiology. Eur Heart J 1998;19:207–229.

Doyley MM. Model-based elastography: A survey of approaches to the inverse elasticity problem. Phys Med Biol 2012;57: R35–R73.

Doyley MM, Mastik F, de Korte CL, Carlier SG, Cespedes EI, Serruys PW, Bom N, van der Steen AFW. Advancing intravascular ultrasonic palpation toward clinical applications. Ultrasound Med Biol 2001;27:1471–1480.

Finet G, Ohayon J, Rioufol G. Biomechanical interaction between cap thickness, lipid core composition and blood pressure in vulnerable coronary plaque: Impact on stability or instability. Coron Artery Dis 2004;15:13–20.

Fleg JL, Stone GW, Fayad ZA, Granada JF, Hatsukami TS, Kolodgie FD, Ohayon J, Pettigrew RI, Sabatine MS, Tearney GJ, Waxman S, Domanski MJ, Srinivas PR, Narula J. Detection of High-Risk Atherosclerotic Plaque: Report of the NHLBI Working Group on Current Status and Future Directions. JACC Cardiovasc Imaging 2012;5:941–955.

Glagov S, Weisenberg E, Zarins CK, Stankunavicius R, Kolettis GJ. Compensatory enlargement of human atherosclerotic coronary arteries. N Engl J Med 1987;316:1371–1375.

Jang IK, Bouma BE, Kang DH, Park SJ, Park SW, Seung KB, Choi KB, Shishkov M, Schlendorf K, Pomerantsev E, Houser SL, Aretz HT, Tearney GJ. Visualization of coronary atherosclerotic plaques in patients using optical coherence tomography: Comparison with intravascular ultrasound. J Am Coll Cardiol 2002;39:604–609.

Kim K, Weitzel WF, Rubin JM, Xie H, Chen X, O'Donnell M. Vascular intramural strain imaging using arterial pressure equalization. Ultrasound Med Biol 2004;30:761–771.

Larose E, Yeghiazarians Y, Libby P, Yucel EK, Aikawa M, Kacher DF, Aikawa E, Kinlay S, Schoen FJ, Selwyn AP, Ganz P. Characterization of human atherosclerotic plaques by intravascular magnetic resonance imaging. Circulation 2005;112:2324–2331.

Le Floc'h S, Cloutier G, Finet G, Tracqui P, Pettigrew RI, Ohayon J. On the potential of a new IVUS elasticity modulus imaging approach for detecting vulnerable atherosclerotic coronary plaques: In vitro vessel phantom study. Phys Med Biol 2010;55:5701–5721.

Le Floc'h S, Cloutier G, Saijo Y, Finet G, Yazdani SK, Deleaval F, Rioufol G, Pettigrew RI, Ohayon J. A four-criterion selection procedure for atherosclerotic plaque elasticity reconstruction based on in vivo coronary intravascular radial strain sequences. Ultrasound Med Biol 2012;38:2084–2097.

Le Floc'h S, Ohayon J, Tracqui P, Finet G, Gharib AM, Maurice RL, Cloutier G, Pettigrew RI. Vulnerable atherosclerotic plaque elasticity reconstruction based on a segmentation-driven optimization procedure using strain measurements: Theoretical framework. IEEE Trans Med Imaging 2009;28:1126–1137.

Libby P. Current concepts of the pathogenesis of the acute coronary syndromes. Circulation 2001;104:365–372.

Libby P, Ridker PM, Maseri A. Inflammation and atherosclerosis. Circulation 2002;105:1135–1143.

Lloyd-Jones D, Adams RJ, Brown TM, Carnethon M, Dai S, De Simone G, Ferguson TB, Ford E, Furie K, Gillespie C, Go A, Greenlund K, Haase N, Hailpern S, Ho PM, Howard V, Kissela B, Kittner S, Lackland D, Lisabeth L, Marelli A, McDermott MM, Meigs J, Mozaffarian D, Mussolino M, Nichol G, Roger VL, Rosamond W, Sacco R, Sorlie P, Stafford R, Thom T, Wasserthiel-Smoller S, Wong ND, Wylie-Rosett J. Executive summary: Heart disease and stroke statistics—2010 update: A report from the American Heart Association. Circulation 2010;121: 948–954.

Loree HM, Kamm RD, Stringfellow RG, Lee RT. Effects of fibrous cap thickness on peak circumferential stress in model atherosclerotic vessels. Circ Res 1992;71:850–858.

Maldonado N, Kelly-Arnold A, Vengrenyuk Y, Laudier D, Fallon JT, Virmani R, Cardoso L, Weinbaum S. A mechanistic analysis of the role of microcalcifications in atherosclerotic plaque stability: Potential implications for plaque rupture. Am J Physiol Heart Circ Physiol 2012;303:H619–H628.

Maurice RL, Fromageau J, Brusseau E, Finet G, Rioufol G, Cloutier G. On the potential of the lagrangian estimator for endovascular ultrasound elastography: In vivo human coronary artery study. Ultrasound Med Biol 2007;33:1199–1205.

Maurice RL, Ohayon J, Finet G, Cloutier G. Adapting the Lagrangian speckle model estimator for endovascular elastography: Theory and validation with simulated radio-frequency data. J Acoust Soc Am 2004;116:1276–1286.

Nozue T, Yamamoto S, Tohyama S, Umezawa S, Kunishima T, Sato A, Miyake S, Takeyama Y, Morino Y, Yamauchi T, Muramatsu T, Hibi K, Sozu T, Terashima M, Michishita I. Statin treatment for coronary artery plaque composition based on intravascular ultrasound radiofrequency data analysis. Am Heart J 2012;163: 191–199.e1.

Ohayon J, Dubreuil O, Tracqui P, Le Floc'h S, Rioufol G, Chalabreysse L, Thivolet F, Pettigrew RI, Finet G. Influence of residual stress/strain on the biomechanical stability of vulnerable coronary plaques: Potential impact for evaluating the risk of plaque rupture. Am J Physiol Heart Circ Physiol 2007;293: H1987–H1996.

Ohayon J, Finet G, Gharib AM, Herzka DA, Tracqui P, Heroux J, Rioufol G, Kotys MS, Elagha A, Pettigrew RI. Necrotic core thickness and positive arterial remodeling index: Emergent biomechanical factors for evaluating the risk of plaque rupture. Am J Physiol Heart Circ Physiol 2008;295:H717–H727.

Ohayon J, Teppaz P, Finet G, Rioufol G. In-vivo prediction of human coronary plaque rupture location using intravascular ultrasound and the finite element method. Coron Artery Dis 2001;12: 655–663.

Ophir J, Cespedes I, Ponnekanti H, Yazdi Y, Li X. Elastography: A quantitative method for imaging the elasticity of biological tissues. Ultrason Imaging 1991;13:111–134.

Richards MS, Doyley MM. Investigating the impact of spatial priors on the performance of model-based IVUS elastography. Phys Med Biol 2011;56:7223–7246.

Rioufol G, Finet G, Ginon I, Andre-Fouet X, Rossi R, Vialle E, Desjoyaux E, Convert G, Huret JF, Tabib A. Multiple atherosclerotic plaque rupture in acute coronary syndrome: A three-vessel intravascular ultrasound study. Circulation 2002;106:804–808.

Tearney GJ, Waxman S, Shishkov M, Vakoc BJ, Suter MJ, Freilich MI, Desjardins AE, Oh WY, Bartlett LA, Rosenberg M, Bouma BE. Three-dimensional coronary artery microscopy by intracoronary optical frequency domain imaging. JACC Cardiovasc Imaging 2008;1:752–761.

Timoshenko SP, Goodier JN. Theory of elasticity. 3rd ed. New York: McGraw-Hill; 1987:13–14, 68–71.

Vancraeynest D, Pasquet A, Roelants V, Gerber BL, Vanoverschelde JL. Imaging the vulnerable plaque. J Am Coll Cardiol 2011;57: 1961–1979.

Virmani R, Burke AP, Farb A, Kolodgie FD. Pathology of the vulnerable plaque. J Am Coll Cardiol 2006;47:C13–C18.

Virmani R, Kolodgie FD, Burke AP, Farb A, Schwartz SM. Lessons from sudden coronary death: A comprehensive morphological classification scheme for atherosclerotic lesions. Arterioscler Thromb Vasc Biol 2000;20:1262–1275.

Wan M, Li Y, Li J, Cui Y, Zhou X. Strain imaging and elasticity reconstruction of arteries based on intravascular ultrasound video images. IEEE Trans Biomed Eng 2001;48:116–120.

Ylä-Herttuala S, Bentzon JF, Daemen M, Falk E, Garcia-Garcia HM, Herrmann J, Hoefer I, Jukema JW, Krams R, Kwak BR, Marx N, Naruszewicz M, Newby A, Pasterkamp G, Serruys PW, Waltenberger J, Weber C, Tokgozoglu L. Stabilisation of atherosclerotic plaques: Position paper of the European Society of Cardiology (ESC) Working Group on Atherosclerosis and Vascular Biology. Thromb Haemost 2011;106:1–19.

APPENDIX I

FORMULATION OF THE ORIGINAL STRESS-STRAIN MODULUS PALPOGRAM

Céspedes et al. (2000) defined the S-SM modulus as the ratio of the average radial stress to the average radial strain along the radial axis

$$E_{\text{palpo}}(\theta) = \frac{\left| \int_{R_i(\theta)}^{R_p(\theta)} \sigma_{rr}(r,\theta)dr \right|}{\varepsilon(\theta)} \tag{A1}$$

where $\varepsilon(\theta)$ is the average radial strain (given by Eq. [1b]); $\sigma_{rr}(r,\theta)$ is the radial stress component; and $R_i(\theta)$ and $R_p(\theta)$ are the non-constant inner and outer radii of the palpography domain (Ω_{paplo}), respectively.

Let us assume that the artery is a thick-walled cylinder (with inner and outer radii R_i and R_o, respectively), isotropic, homogeneous, incompressible, linearly elastic (with Young's modulus E), submitted to uniform pressure (ΔP) on the inner boundary $r = R_i$ and zero pressure on the outer boundary $r = R_o$. By assuming plane strain condition and by considering a concentric circular palpography domain Ω_{palpo} (with $R_i \leq r \leq R_p$), the spatial distribution of the local S-SM (given by Eq. [A1]) becomes constant through Ω_{palpo} and equal to

$$E_{\text{palpo}}^{\text{cylinder}} = \frac{\Delta P \left| \int_{R_i}^{R_p} g(r)dr \right|}{\varepsilon} \tag{A2}$$

with

$$\varepsilon = \frac{3}{2E}\frac{\alpha_o^2}{\alpha_p\left(\alpha_o^2-1\right)}\Delta P \tag{A3a}$$

$$\int_{R_i}^{R_p} g(r)dr = \frac{\left(\alpha_o^2-\alpha_p\right)}{\alpha_p\left(\alpha_o^2-1\right)} \tag{A3b}$$

where the constant ε is the absolute value of the compressive average radial strain (with amplitude given by Eq. [A3a]); and α_o and α_p are the relative thicknesses of the arterial wall and palpography domain Ω_{palpo}, respectively ($\alpha_o = R_o/R_i$ and $\alpha_p = R_p/R_i$). The spatial function $g(r)$ is a correcting shape function that accounts for the geometry of the thick-walled cylindrical artery. For a specific circular palpography domain only (*i.e.,* when $R_p = [2\alpha_o^2/(\alpha_o^2+1)]R_i$), the amplitude of the uniform local S-SM becomes:

$$E_{\text{palpo}}^{\text{cylinder}*} = \frac{\Delta P/2}{\varepsilon} \tag{A4}$$

It is interesting to note that this S-SM (*i.e.*, $E_{palpo}^{\text{cylinder}*}$) is not the Young's modulus E of the isotropic concentric plaque, because by substituting Eq. (A3a) into Eq. (A4) we obtain the relationship

$$E_{\text{palpo}}^{\text{cylinder}*} = \frac{1}{3}\frac{\alpha_p\left(\alpha_o^2-1\right)}{\alpha_o^2}E \tag{A5}$$

An exact analytical S-SM formula is difficult to derive for heterogeneous, eccentric and complex plaque geometries. Céspedes et al. (2000) were inspired by the simplified S-SM solution obtained for a thick-walled cylindrical vessel (Eq. [A4]) to propose their S-SM approximation given by Eq. (1a).

APPENDIX II

CONVERTING OUR WHITE NOISE INTO DECIBELS

To find correspondence between the imposed white noise and the signal-to-noise ratio (SNR, in dB), we used the relationship

$$\text{SNR} = 10\log_{10}\left(\frac{A_{\text{signal}}^2}{A_{\text{noise}}^2}\right) \tag{A6}$$

where A_{signal} and A_{noise} are the signal and noise amplitudes, respectively. We identified the signal amplitude A_{signal} to the mean spatial strain amplitude free of noise. Moreover, in our study, we used the following normal distribution of noise A_{noise} with zero mean and standard deviation $\sigma(r,\theta) = (a\varepsilon_{rr}(r,\theta)+b)\beta$, where $a = 0.2\%$, $b = 0.04\%$ and β varies from 2 to 6 (Baldewsing et al. 2005; Le Floc'h et al. 2009):

$$A_{\text{noise}}(r,\theta) = \text{Normal}\left(0,\sigma(r,\theta)^2\right) \tag{A7}$$

By considering these two expressions of A_{signal} and A_{noise}, we found that

$$\text{SNR} = 10\log_{10}\left(\frac{\sum_{r,\theta}\left[\varepsilon_{rr}(r,\theta)\right]^2}{\sum_{r,\theta}\left[A_{\text{noise}}(r,\theta)\right]^2}\right) \tag{A8}$$